



A Thin Skin Calorimeter (TSC) for quantifying irradiation during large-scale fire testing



Juan P. Hidalgo^{a, b, *}, Cristian Maluk^{a, b}, Adam Cowlard^{a, c}, Cecilia Abecassis-Empis^{a, c}, Michal Krajcovic^a, José L. Torero^b

^a School of Engineering, The University of Edinburgh, Edinburgh, EH9 3JL, UK

^b School of Civil Engineering, The University of Queensland, Brisbane St Lucia, QLD, 4072, Australia

^c TAEC, Edinburgh, EH16 5AA, UK

ARTICLE INFO

Article history:

Received 3 September 2015

Received in revised form

21 October 2016

Accepted 21 October 2016

Available online 9 November 2016

Keywords:

Thin skin calorimeter

Irradiance

Incident radiant heat flux

Compartment fire tests

Thermal boundary condition

Heat transfer

Fire safety design

ABSTRACT

This paper details a novel method for quantifying irradiation (incident radiant heat flux) at the exposed surface of solid elements during large-scale fire testing. Within the scope of the work presented herein, a type of Thin Skin Calorimeter (TSC) was developed intending for a practical, low cost device enabling the cost-effective mass production required for characterising the thermal boundary conditions during multiple large-scale fire tests. The technical description of the TSC design and a formulation of the proposed calibration technique are presented. This methodology allows for the quantification of irradiation by means of an *a posteriori* analysis based on a temperature measurement from the TSC, a temperature measurement of the gas-phase in the vicinity of the TSC and a correction factor defined during a pre-test calibration process. The proposed calibration methodology is designed to account for uncertainties inherent to the simplicity of the irradiation measurement technique, therefore not requiring precise information regarding material thermal and optical properties. This methodology is designed and presented so as to enable adaption of the technique to meet the specific requirements of other experimental setups. This is conveyed by means of an example detailing the design and calibration of a device designed for a series of large-scale experiments as part of the 'Real Fires for the Safe Design of Tall Buildings' project.

© 2016 The Authors. Published by Elsevier Masson SAS. This is an open access article under the CC BY license (<http://creativecommons.org/licenses/by/4.0/>).

1. Introduction & background

Design for fire safety in the built environment is fundamentally based upon the design fire(s) defined by the practitioner charged with addressing fire safety considerations during design. The design fire(s) ought to represent potential fire scenarios for assessing the performance of structural (load bearing) and/or non-structural (compartmentation) elements, whilst attempting to account for the possible influences of the temporal and spatial evolution of the fire. Commonly, prescribed fully-developed design fires assume homogenous conditions inside a compartment [1,2], and are classically defined as gas-phase time-temperature curves (i.e. time-histories of gas temperature inside a compartment in fire).

The belief that uniform burning inside the fire compartment, and therefore uniform temperature distribution, results in the most severe conditions for structural fire has been scrutinised by several authors [3,4]. As a result, recent studies have focused their efforts on defining temporally and spatially non-uniform design fires [5,6].

The scientific community is confronting the problems associated with a lack of scientific and practical understanding of compartment fires outside the classic quasi-cubic compartment framework [4]; research projects towards large-scale compartment fire testing for systematic research of the fire phenomenon, and for validation of available empirical correlations and computational models, are thus experiencing something of a renaissance (e.g. Refs. [7,8]).

The heat transferred from the fire environment onto compartment elements (structural and non-structural) is determined by the net/total heat flux at the surface (q''_{net}) [9,10], which is classically expressed by Fourier's law:

* Corresponding author. School of Civil Engineering, The University of Queensland, Brisbane St Lucia, QLD, 4072, Australia.

E-mail address: j.hidalgo@uq.edu.au (J.P. Hidalgo).

Nomenclature		Greek letters	
A	surface area (m^2)	α	absorptivity (–)
C	thin skin calorimeter correction factor (–)	δ	thickness (m)
c_p	specific heat capacity ($\text{kJ} \cdot \text{kg}^{-1} \cdot \text{K}^{-1}$)	ε	emissivity (–)
E_{disc}	emissive power from the TSC metallic disc surface ($\text{W} \cdot \text{m}^{-2}$)	ν	kinematic viscosity ($\text{m}^2 \cdot \text{s}^{-1}$)
F	view factor (–)	κ	extinction coefficient (m^{-1})
Gr	Grashof number (–)	ρ	density ($\text{kg} \cdot \text{m}^{-3}$)
h_c	convective heat transfer coefficient ($\text{W} \cdot \text{m}^{-2} \cdot \text{K}^{-1}$)	σ	Stefan–Boltzmann constant ($\text{W} \cdot \text{m}^{-2} \cdot \text{K}^{-4}$)
J	radiosity ($\text{W} \cdot \text{m}^{-2}$)	<i>Subscripts</i>	
k	thermal conductivity ($\text{W} \cdot \text{m}^{-1} \cdot \text{K}^{-1}$)	<i>air</i>	of the air
L	characteristic length or path length (m)	<i>amb</i>	of the ambient or fluid
\overline{Nu}_L	Nusselt number (–)	<i>disc</i>	of the thin skin calorimeter metallic disc
Pr	Prandtl number (–)	<i>g</i>	of the gas
\dot{q}_{cond}''	conductive heat flux from the TSC metallic disc to the insulation core ($\text{W} \cdot \text{m}^{-2}$)	L	of the characteristic length or boundary layer
$\dot{q}_{stor.disc}''$	stored heat flux in the TSC metallic disc ($\text{W} \cdot \text{m}^{-2}$)	r	of the reference black body with a view factor equal to one
\dot{q}_{conv}''	convective heat flux ($\text{W} \cdot \text{m}^{-2}$)	s	of the surface
\dot{q}_{net}''	net heat flux or total heat flux ($\text{W} \cdot \text{m}^{-2}$)	∞	of the surroundings
Ra_L	Rayleigh number (–)	<i>Acronyms</i>	
t	time (s)	FRTD 4	wire resistance temperature detector
T	temperature (K or °C)	H-TRIS	heat transfer rate inducing system
		PT	plate thermometer
		TSC	thin skin calorimeter

$$\dot{q}_{net}'' = -k \cdot \left. \frac{\delta T}{\delta x} \right|_s \quad (1)$$

where k is the thermal conductivity of the material and $\left. \frac{\delta T}{\delta x} \right|_s$ is the thermal gradient at the surface.

Quantification of the thermal boundary condition, that determines the net heat flux, tends to be described by using gas-phase (or other) temperature measurements and by assuming a series of prescribed heat transfer coefficients (e.g. surface absorptivity, emissivity, convective heat transfer, and/or view factors), representative of the fire environment. This boundary condition is commonly expressed as:

$$\dot{q}_{net}'' = \varepsilon \cdot \sigma \cdot (T_r^4 - T_s^4) + h_c \cdot (T_g - T_s) \quad (2)$$

where ε is the emissivity of the material, σ is the Stefan-Boltzmann constant, h_c is the convective heat transfer coefficient, T_r is the black body reference temperature assuming a view factor as unity, T_g is the gas-phase temperature, and T_s is the surface temperature. It should be noted that this expression considers the emissivity and absorptivity to be equal.

Despite the fact that past research studies have derived numerous empirical and theoretical correlations between temperature inside the compartment (e.g. gas-phase temperature) and net heat flux [11], large uncertainty still exists when quantifying the thermal boundary condition (i.e. net/total heat flux) at the exposed surface of solid elements during a compartment fire [12]. These uncertainties are mainly associated with:

- Assumptions considering uniform temperatures in the compartment, and therefore uniform heat flux distributions onto the solid elements.
- Errors in the measurement of the gas-phase temperature, due to radiative effects on the thermocouple bead [7].

- Undetermined heat transfer coefficients, such as emissivity and absorptivity (dependent on material properties) and convective coefficient (dependent on the local flow field and characteristic length of the solid).
- Assumptions considering an optically thick environment (i.e. $\kappa L \gg 1$, with κ the extinction coefficient and L the path length), thus disregarding attenuation of the radiant intensity by transmission, and considering the black body reference temperature for radiation exchange as the gas-phase temperature with a view factor as unity.

The majority of these assumptions are particularly incompatible with spatially variable fires, therefore uncertainty associated to heat transfer coefficients is further magnified. Research has demonstrated that significant spatial variation of incident heat flux can exist over an internal surface of a fire compartment, even in compartments of similar dimensions to those used to define classical *Regime I* compartment fire dynamics [13]. Further development of the knowledge base surrounding spatially variable compartment fires will necessitate a high resolution characterisation of the distribution of irradiance to the solid boundaries during large-scale experimentation. Experimentation with measurements at an appropriate resolution will enable further crucial research such as the validation of computational models, which requires a data point density suitable for comparing the spatial and temporal variation of the parameters of interest between the fire test and the models [4,14].

1.1. Research significance

Performing a practical, yet accurate, quantification of the thermal boundary condition at a functional resolution during a large-scale compartment fire experiment presents a major challenge thus there is a clear need for a robust and low cost device to measure irradiation (i.e. incident radiant heat flux). This paper

details the design, construction and calibration of a measurement device intended for this purpose. The device and thus measurement technique developed is by necessity simple, keeping costs low and thus enabling mass production. This enables experiments with greater sensor resolution, even accounting for destruction of sensors over the course of multiple experiments. The technique has been developed iteratively, initially for both small [15–17] and large-scale experimentation [18], and revised more recently for large-scale experimentation [14]. Results from large-scale experiments in particular [14,18] demonstrate the level of distribution of irradiance within real-scale compartments and thus the significance of the development of TSCs for this purpose.

In the following sections, an introduction to common gauges for measuring heat flux is presented (section 2), proceeded by an in-depth description of the Thin Skin Calorimeter gauge and the derivation of the formulation that is used to quantify irradiation (section 3). A calibration procedure is then detailed in section 4, including an analysis of the uncertainties intrinsic to using this gauge and the development of a novel methodology based on a calibration factor. The outcomes from a calibration process for a specific Thin Skin Calorimeter are presented and discussed, leading to the derivation of a calibration function. Eventually, the methodology is validated by exposing the calibrated Thin Skin Calorimeter to a series of predefined irradiation-time curves, representing different likely fire scenarios.

2. Gauges for measuring heat flux

The measurement of heat flux is not a new thing; past research studies have yielded numerous methods and instruments for gauging net/total heat flux resulting from the fire in a compartment (e.g. Refs. [18,20]). These measurements of net/total heat flux, although not being applicable to the compartment elements as a boundary condition due to the dependency to the material properties of the element [21], have served as a method to standardise the conditions of heat exposure in fire testing. Additionally, they provide a series of quantities that can be used for model validation.

Within the context of the abovementioned applications (experimental fire testing), the calorimeters are frequently used for measuring incident radiant heat flux at the exposed surface of solid elements. Numerous techniques have been developed for gauging the thermal boundary condition at the exposed surface of heated solid elements [19–28], although this continually contains uncertainty associated with the assumptions made to define the thermal boundary condition (e.g. absorptivity and heat transfer coefficients). The following sections examines two widely used irradiation measuring instruments presented within the fire (and broader) scientific community: the water-cooled heat flux gauge and the plate thermometer.

2.1. Water-cooled heat flux gauges

Water-cool heat flux gauges quantify total heat flux by measuring the temperature difference within a reference material [18,20]. The unexposed surface of the reference material is water-cooled, hence maintained at low ambient temperature. Water-cooled heat flux gauges are pre-calibrated using a reference heat flux meter [26], and as a result incident radiant heat flux is correlated to the temperature difference dependency, monitored as a voltage output. If conditions in the boundary layer during fire testing and during calibration are equivalent (i.e. negligible or no convective heat transfer taking place), the incident radiant heat flux can be directly measured during fire testing conditions. In the case that different flow conditions are observed, a correction must be taken into account in order to provide quantification of the incident

radiant heat flux [27]. Water-cooled heat flux gauges are relatively delicate and expensive instruments, thus hindering their use in large-scale fire testing applications which require a high instrumentation density.

For a system in which the control variable is defined as the incident radiant heat flux (\dot{q}_{inc}'') at the exposed surface of the solid, the local energy conservation equation can be expressed as:

$$\dot{q}_{net,s}'' = \alpha_s \dot{q}_{inc}'' - \dot{q}_{losses}'' \quad (3)$$

where the net heat flux ($\dot{q}_{net,s}''$) is calculated accounting for the absorptivity (α_s) and heat losses (\dot{q}_{losses}'') at the exposed surface of the solid. Hence, the time-history of incident radiant heat flux (\dot{q}_{inc}'') is an independent control variable. The heat flux losses at the specimen's exposed surface may be calculated using a direct heat transfer model (analytical or numerical, implicit or explicit).

2.2. Thin skin calorimeters (TSCs)

Thin Skin Calorimeters (TSCs) are one of many instruments used for gauging (i.e. measuring) heat transfer rates (total heat flux), and allows for the quantification of the incident radiant heat flux at the exposed surface of solid elements (e.g. structural elements) during a fire test [28]. Thin Skin Calorimeters have been largely implemented in large-scale compartment fire tests [14,18,29–31] and in full-scale outdoor experiments such as wildland fire tests [32]. The following sections thoroughly examine the technical and theoretical aspects of the TSC, and the methodology to quantify irradiation.

Thin Skin Calorimeters are based on the concept of a lumped capacitance (described in the following section), obtained by the conjugation of two materials with largely opposed thermal properties and thickness; traditionally achieved by using a thin metallic disc/plate attached to a thick insulation core (refer to Fig. 1). This principle allows for assuming a uniform temperature through the thickness of the metallic disc, measured by a thermocouple placed at its rear surface (i.e. unexposed surface). The assumption of the metallic plate acting as a thermally thin element is satisfied by verifying that the Biot number is below 0.1; easily attainable if a sufficiently thin metallic disc is used [9]. Additionally, the metal and insulation material used to build TSCs must meet resistance conditions to thermal decomposition, and absence of major endothermic or exothermic reactions for the temperature range of applicability.

2.2.1. The plate thermometer

The plate thermometer is essentially one specific type of TSC [33]. For the plate thermometer, the concept of lumped capacitance is obtained by the conjugation of a $100 \times 100 \text{ mm}^2$ and 0.7 mm thick nickel alloy steel plate, insulated on the rear side with an inorganic insulation material with a density of $280 \pm 30 \text{ kg/m}^3$ [33]; a thermocouple is welded to the unexposed surface of the steel plate.

In the late 1990s, the plate thermometer was adopted by European (and other) regulations on standard fire resistance testing for controlling and measuring the temperature inside standard furnaces. Plate thermometers are intended to be placed near the test exposed surface of the specimen, facing the source of heat (i.e. flames from the fire, hot gases or/and surfaces), thereby receiving the same irradiation as the surface [34].

The thermal boundary conditions at the exposed surfaces of a solid depends on the thermal state at the exposed surfaces, hence on the thermal properties (i.e. thermal inertia) of the solid being heated. Adoption of the plate thermometer as the standard gauge for temperature control within testing furnaces is also, and

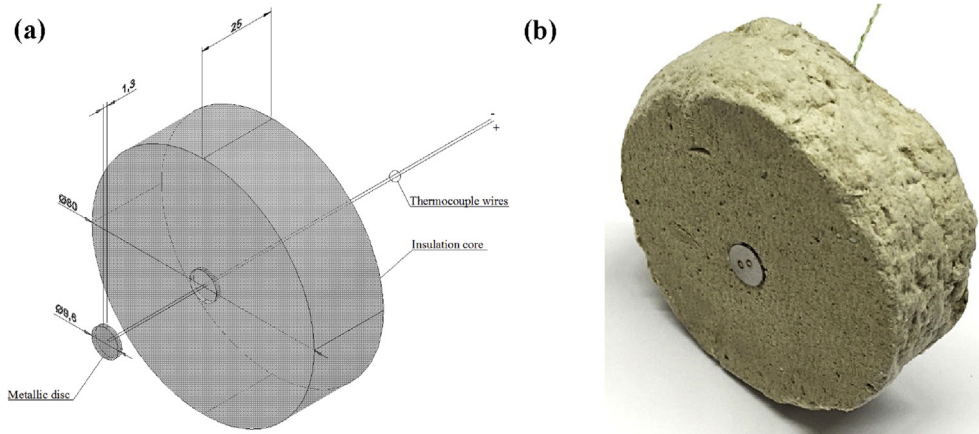


Fig. 1. Thin Skin Calorimeter based on a 25 mm thick insulation core and a 1.3 mm thick stainless steel disc: (a) Exploded sketch (b) Real assembled TSC.

inevitably, governed by energy conservation inside the control volume [35].

3. A thin skin calorimeter (TSC) for large-scale fire testing

A Thin Skin Calorimeters designed and built within the scope of this work, and used for a series of large-scale fire compartment experiments as part of the project ‘Real Fires for the Safe Design of Tall Buildings’ [14] is presented in this section.

3.1. Technical description

This TSC consists of a 25 mm thick Superwool[®] HT disc (herein referred to as insulation core) and a 1.3 mm thick 304b stainless steel disc (herein referred to as metallic disc). The diameter of the insulation core and the metallic disc are 80 mm and 9.6 mm, respectively. The two wires of a K-type thermocouple are welded to the back surface of the metallic disc, separated by a distance of approximately 1 mm (refer to Fig. 2). As shown in Fig. 1, the metallic element is embedded onto the surface of the insulation core, so as to achieve a flush surface at the exposed face. The thermocouple wires welded to the back surface of the metallic disc are passed through the core of the insulation and finally connected to a data logger.

A summary of the assumed thermo-physical properties of the materials used for the fabrication of this particular TSC are presented in Table 1. While the specific materials used for the TSC presented here may provide good results, other materials that satisfy the abovementioned conditions could be used for preparing TSCs. Indeed, one of the main advantages of these devices is the flexibility and reduced cost of fabrication, and lack of need for

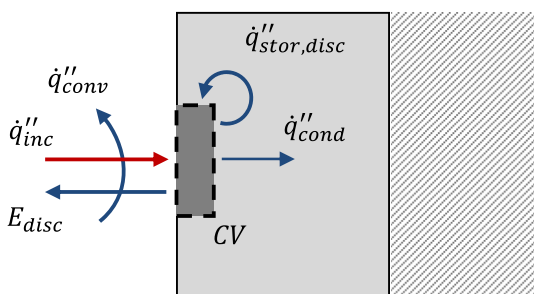


Fig. 2. Heat balance at the surface of the thin skin calorimeter.

precise determination of material properties.

3.2. Theoretical quantification of incident radiant heat flux

The methodology developed to quantify the incident radiant heat flux using a TSC requires solving the energy balance at the control volume of the metallic disc, and characterising the heat losses at the unexposed surfaces (rear and edges) of the metallic disc. The approach described herein uses a correction factor C integrated into the conduction term so as to overcome the uncertainty in the quantification of material properties from the metallic disc such as absorptivity, emissivity and heat capacity.

Despite the fact that available guidelines for the design of TSCs [28] and previous works [16,29] have demonstrated the success of this technique, there are a lack of studies presenting (1) a methodology for determining actual levels of irradiance based on the use of the TSC, and (2) an assessment of the different uncertainties from this methodology.

Similarly to the other aforementioned instruments, the use of TSCs can provide a quantification of the net/total heat flux absorbed by the instrument. Thereafter, a quantification of the incident radiant flux (irradiation) received at the exposed surface of the solid elements (i.e. solid boundaries of the thermodynamic system being studied) can be determined by an *a posteriori* analysis. The thermal boundary condition, however, is not only determined by incident irradiation, but also by the gas-phase temperature and the gas flow surrounding the exposed, solid surface (boundary layer). Therefore, if a precise boundary condition definition is required, further analysis on the convective heat transfer coefficient must be pursued. This is out of the scope of the work presented herein; further information about the determination of the convective heat flux can be found elsewhere [36].

The incident radiant heat flux impinging onto the exposed surface of a TSC (\dot{q}''_{inc}) can be calculated by performing an energy balance at the control volume (CV) of the disc, schematically represented in Fig. 2, and formulated in Eq. (4):

$$\alpha_{disc} \cdot \dot{q}''_{inc} + \dot{q}''_{conv} = \dot{q}''_{stor,disc} + E_{disc} + \dot{q}''_{cond} \quad (4)$$

where α_{disc} is the absorptivity of the metallic disc component of the TSC, \dot{q}''_{conv} is the convective heat flux at the exposed surface of the metallic disc, \dot{q}''_{cond} is the conductive heat flux from the metallic disc to the insulation core, $\dot{q}''_{stor,disc}$ is the stored heat flux in the metallic disc, and E_{disc} is the radiant heat flux emitted by the surface of the metallic disc (hemispherical emissive power). These terms are

Table 1

Assumed temperature (T) dependent thermo-physical properties of the insulation core (Superwool® HT) and the metallic disc (304b stainless steel) used for construction of a TSC.

Material	Thermal conductivity /W m ⁻¹ K ⁻¹	Density /kg m ⁻³	Specific heat capacity /J kg ⁻¹ K ⁻¹	Emissivity /-
Superwool® HT	0.05 at 200 °C 0.08 at 400 °C 0.11 at 600 °C 0.15 at 800 °C 0.20 at 1000 °C	350 at 20 °C	1220 at 20 < T < 1000 °C	Unknown
304b stainless steel	15 at 200 °C 18 at 400 °C	7800 at 20 < T < 1000 °C	450 + 0.28 · T - 2.91 · 10 ⁻⁴ · T ² + 1.34 · 10 ⁻⁷ · T ³ at 20 < T < 1000 °C (T in °C)	216 °C–490 °C 0.44 to 0.36 (generic 304)

further described below.

This formulation lumps the received irradiation (deducting any absorption from the semi-transparent media) from the various sources such as smoke, hot surfaces and/or luminous flames into one parameter, the effective irradiation or incident radiant heat flux (\dot{q}_{inc}'').

The heat flux stored by the disc can be determined as a function of its temperature variation:

$$\dot{q}_{stor, disc}'' = \frac{m_{disc}}{S_{disc}} \cdot c_p \cdot \frac{dT_{disc}}{dt} \quad (5)$$

where m_{disc} , S_{disc} and c_p are the mass, surface area and specific heat capacity of the material of the metallic disc respectively, and $\frac{dT_{disc}}{dt}$ is its temperature variation over time.

The emitted radiation from the disc can be calculated as noted in Eq. (6), which reflects the rate per unit area at which radiation is emitted at all possible directions and wavelengths:

$$E_{disc} = \varepsilon_{disc} \cdot \sigma \cdot T_{disc}^4 \quad (6)$$

where ε_{disc} is the emissivity of the disc surface, σ is the Stefan–Boltzmann constant, and T_{disc} the temperature within the disc.

The convective heat flux can be evaluated by applying Newton's law of cooling, estimating the convective heat transfer coefficient (h_c) and measuring the temperature of the gas flow at the immediate vicinity of the sensor surface (T_g):

$$\dot{q}_{conv}'' = h_c \cdot (T_g - T_{disc}) \quad (7)$$

with the convective heat transfer coefficient estimated by calculating the Nusselt number, defined as:

$$\overline{Nu}_L = \frac{h_c \cdot L_c}{k_g} \quad (8)$$

where L_c is the characteristic length and k_g is the thermal conductivity of the gas. Different correlations can be used for estimating the Nusselt number, depending on the conditions of the flow, i.e. external forced flow or natural convection. Several empirical expressions are commonly used for evaluating free convection conditions (cooling) as a function of the Rayleigh number, while conditions of forced flow require the characterisation of the Reynolds number.

The conductive heat flux from the disc onto the insulation core depends on the relative difference of thermal properties of the metallic disc and the insulation core. Since this term is expected to be relatively low in comparison to the other energy terms due to the low thermal conductivity of the insulation core, the approach proposed by the authors is to consider the conductive heat flux as a fraction of the absorbed incident radiant heat flux. This assumption seems robust as essentially the obtained net heat flux is caused by

external sources of incoming energy (incident radiation and/or hot gases). Therefore, the conductive heat flux can be expressed as:

$$\dot{q}_{cond}'' = C \cdot \alpha_{disc} \cdot \dot{q}_{inc}'' \quad (9)$$

where C is the conduction factor, which hereafter will be denoted as correction factor. Indeed, as will be presented in the following section, this particular definition allows overcoming certain uncertainties by using a calibration procedure. The reduced fraction of energy transferred to the insulation core where the metallic plate is embedded has been demonstrated by previous authors [16,29,37].

Taking Eqs. (5)–(9), the heat balance in the control volume noted in Eq. (4) can be rewritten as the following expression:

$$\alpha_{disc} \cdot \dot{q}_{inc}'' + h_c \cdot (T_g - T_{disc}) = C \cdot \alpha_{disc} \cdot \dot{q}_{inc}'' + \frac{m_{disc}}{S_{disc}} \cdot c_p \cdot \frac{dT_{disc}}{dt} + \varepsilon_{disc} \cdot \sigma \cdot T_{disc}^4 \quad (10)$$

Rearranging terms, the incident radiant heat flux can eventually be obtained as:

$$\dot{q}_{inc}''(T_{disc}) = \frac{1}{\alpha_{disc} \cdot (1 - C)} \cdot \left[\frac{m_{disc}}{S_{disc}} \cdot c_p \cdot \frac{dT_{disc}}{dt} + \varepsilon_{TSC} \cdot \sigma \cdot T_{disc}^4 + h_c \cdot (T_{disc} - T_g) \right] \quad (11)$$

As presented in Eq. (11), the incident radiant heat flux can be approximated as a function of the temperature of the metallic disc. This definition suggests that the correction factor is necessarily a function of the temperature of the disc as well, i.e. $C=C(T_s)$. This assumption will be further discussed in the following section.

Due to the low surface area of the disc, and therefore the low contribution to the net radiative exchange of energy with the surroundings, the irradiation can be considered as a parameter independent from the instrument. However, the convective heat transfer is dependent on the temperature of the disc and the development of the boundary layer at its surface. Therefore, despite the fact that the total incident heat flux could be estimated (considered as absorbed radiation plus convection), the application of this term to other elements exposed to the conditions of the fire is fundamentally incorrect due to the dependency of the convective heat flux to the element surface temperature and characteristic length, and the likely different absorptivity.

4. TSC calibration procedure

4.1. Calibration set-up

The calibration of a TSC relies on determining the correction factor as a function of the disc temperature by imposing it to known levels of irradiation, which could be characteristic of real

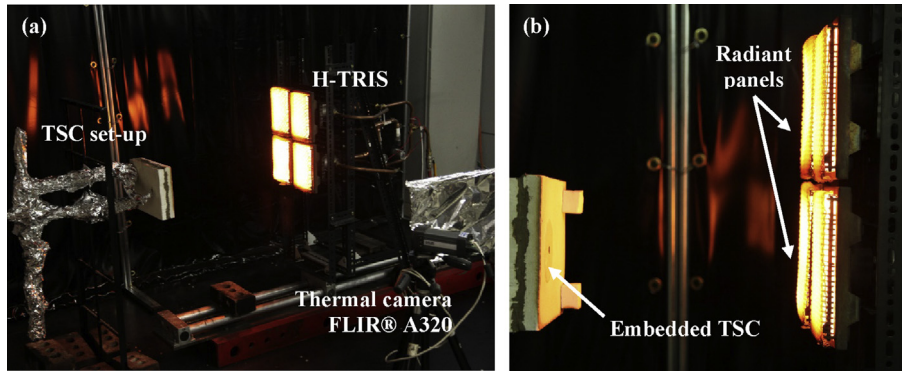


Fig. 3. (a) Set-up for TSC calibration (b) TSC being exposed to radiant heat from H-TRIS [35].

fires. The method used herein corresponds to the use of a series of mobile radiant panels; a Heat-Transfer Rate Inducing System (H-TRIS) test method for which the irradiation is defined as a function of the relative distance between the surface of the panels and the tested sample [35], calibrated against a Schmidt-Boelter gauge [21]. This system allows for the direct control of potentially any predefined time-history of incident radiant heat flux at the exposed surface of essentially any material. The set-up used for the calibration of the previously described TSC is shown in Fig. 3. For ease of calibration, the TSC was embedded within a 20 mm by 20 mm Superwool® HT insulation board, which was supported by a steel frame. The two K-type thermocouple wires were connected to an Agilent 34980A data logger, and a 4-wire resistance temperature detector (FRTD) was used as external reference temperature.

As shown in Fig. 3, the particular calibration set-up used by the authors corresponds to a vertical hot plate orientation, which has been studied extensively by the community [9]. Then, empirical correlations are expected to provide a reasonable quantification of the free convection.

During the calibration process of the TSC, H-TRIS was programmed to impose a time-history of incident radiant heat flux from 10 kW m^{-2} up to 90 kW m^{-2} with steps of 10 kW m^{-2} as shown in Fig. 4. Additionally, a second calibration is performed by stepping down the radiant heat flux with steps of 10 kW m^{-2} after the maximum heat flux of 90 kW m^{-2} is achieved.

Two TSCs are calibrated in order to check the consistency of the results with respect to the fabrication of the instrument.

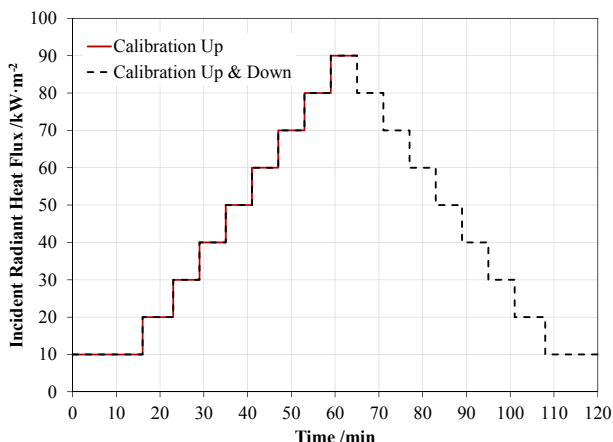


Fig. 4. Time-history of the incident radiant heat flux used for calibration of the TSC.

Additionally, calibrations are repeated twice so as to check the consistency of the results after a first use of the TSC, thus verifying that any possible endothermic or exothermic reaction in the metallic disc or insulation core can be neglected. This procedure is of significant relevance, since it will be demonstrated that the repeated use of TSCs for a series of experimental fire exposures provides consistent and reliable results.

4.2. Sources of uncertainties

A series of uncertainties are encountered when applying the proposed methodology to determine incident radiant heat flux based on the use of TSCs. These uncertainties caused by the inaccurate quantification of the different terms from the energy balance defined in Eq. (4). A description of the different sources of uncertainty is presented below:

4.2.1. Convective heat transfer coefficient

While empirical correlations of the Nusselt number may provide a sensible estimation of the heat transfer coefficient for cooling conditions during calibration, the calculation of this term in a real experiment represents the main uncertainty of the methodology presented herein.

For the particular case of the calibration, an erratic estimation of the heat losses by convection is to be expected if the boundary layer established at both, the surface of radiant panels and TSC, get too close as shown in Fig. 5b. In order to avoid an erratic estimation of the convection during calibration, the calibration procedure is performed in a way such that the relative distance between the surface of the radiant panels and the TSC is higher than a critical thickness. This is conservatively considered as twice the thickness

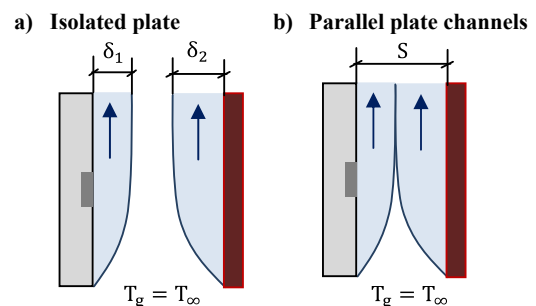


Fig. 5. Schematics of the boundary layer from TSC and radiant panel. Case (a): Cooling conditions from the TSC can be considered as free convection (Eq. (14)). Case (b): Cooling conditions from the TSC are affected by the boundary layer from the radiant panels.

of the boundary layer established at the surface of the radiant panels. Fig. 6 shows an estimation of the boundary layer thickness for a surface at 1200 °C and a surface at the metallic disc temperature obtained from calibration. The maximum thermal boundary layer thickness (δ_L) is approximated according to the following expression given by Incropera et al. [9] for a vertical plate at uniform temperature:

$$\delta_L \approx \frac{6 \cdot L}{\left(\frac{Gr_L}{4}\right)^{1/4}} \quad (12)$$

where L is the length of the vertical plate and Gr_L is the Grashof number.

Fig. 6 shows that the calculated maximum boundary layer thickness for a 300 mm vertical flat plate at 1200 °C is approximately 30–35 mm, while the maximum thickness for the 200 mm assembly during calibration is approximately 25 mm. Therefore, a safe distance of 70 mm between the gauge and the panels is considered for the calibration of the TSCs, which for the particular calibration of the radiant panels approximately corresponds to a radiant incident heat flux of 90 kW m⁻².

4.2.2. Reference incident radiant heat flux

The calibration of the TSC depends on reliable calibrated irradiation levels from the radiant panels at specific relative distances. The use of the Schmidt-Boelter gauge allows to overcome the quantification of transfers of energy by radiation considering view factors. However, the quantification of incident radiant heat flux during the calibration process counts on considering a constant temperature of the panels. Therefore, the reliability of the levels of irradiance resides on verifying that (1) the cooling conditions of the panels are unaffected and (2) the radiation from the tested sample does not alter the temperature of the panels. The former can be satisfied by restricting the relative distance between the panel and the tested sample to twice the boundary layer of the panel. The latter is expected not to be significant due to the low surface area of the tested TSC.

4.2.3. Radiative properties from the disc

The absorptivity and emissivity of the metallic disc determine the absorbed radiant heat flux and the emitted radiation, respectively. Despite some generic values of emissivity for stainless steel 304 are given in Table 1, its dependency with temperature is unknown. Furthermore, it cannot be guaranteed that the Kirchhoff's

law for grey surfaces apply, i.e. absorptivity and emissivity being independent of wavelength over the spectral regions of surface irradiation and emission [9], and therefore $\alpha_{disc} \neq \epsilon_{disc}$. Despite the given uncertainty in characterising the radiative properties of the disc, the use of the correction factor can compensate in first instance an inaccurate selection of the absorptivity, and also a variation of the emissivity with temperature.

4.2.4. Heat capacity from the disc

The stored heat flux term depends on the specific heat capacity and areal density of the disc. Similarly to the radiative properties, generic values of specific heat capacity are provided for stainless steel. However, different quantification of specific heat capacity are provided for different alloys, also dependent on temperature. A factor γ that compensates the uncertainty in the definition of the heat capacity is introduced in the formulation of the energy balance equation presented in the following section.

5. Formulation for the correction factor calibration

The energy balance expression during calibration is analogous to the energy balance defined as in Eq. (4), assuming that the total irradiation measured by the Schmidt-Boelter gauge includes the irradiation received from the surface of the radiant panels and from the surroundings at ambient temperature. Therefore, rearranging terms in Eq. (4), the correction factor C can be defined as:

$$C(T_{disc}) = \frac{\alpha_{disc} \cdot \dot{q}_{inc}'' - [\dot{q}_{stor,disc}(T_{disc}) + E_{disc}(T_{disc}) - \dot{q}_{conv}''(T_{disc})]}{\alpha_{disc} \cdot \dot{q}_{inc}''} \quad (13)$$

Since the calibration is set up with the TSC in a vertical position and at ambient temperature, thus under conditions of cooling by free convection, the convective heat transfer coefficient is calculated considering the empirical correlation of the Nusselt number given by Churchill and Clu [38] for the vertical hot plate considering a laminar flow:

$$\overline{Nu}_L = 0.68 + \frac{0.670 \cdot Ra_L^{1/4}}{\left[1 + \left(\frac{0.492}{Pr}\right)^{9/16}\right]^{4/9}} \quad \text{for any } Ra_L \leq 10^9 \quad (14)$$

where Pr is the Prandtl number and Ra_L is the Rayleigh number that can respectively be expressed as:

$$Ra_L = \frac{g \cdot \beta \cdot (T_S - T_g) \cdot L_c^3}{\nu \cdot \alpha} \quad (15)$$

$$Pr = \frac{\nu}{\alpha} \quad (16)$$

where g is the gravity acceleration, β is the inverse of the film temperature defined as $\beta = 2/(T_S + T_g)$, T_S is the surface temperature, T_g is the fluid temperature, L_c is the characteristic length and ν and α are the kinematic viscosity and thermal diffusivity of the fluid.

Eq. (13) considers the correction factor as temperature dependent since the stored heat, radiative and convective fluxes identified on the right-hand side of the equation are temperature dependent. However, the incident radiant heat flux for the calibration has been defined as a series of constant steps. Then, it is expected a transient and a quasi-steady state regime in the temperature evolution of the disc, and thus the evolution of the stored heat, radiative and convective fluxes. During the transient state the

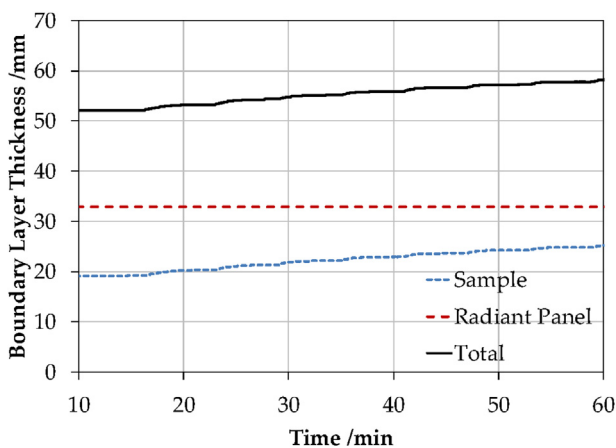


Fig. 6. Calculated boundary layer thickness for tested and radiant panels during calibration.

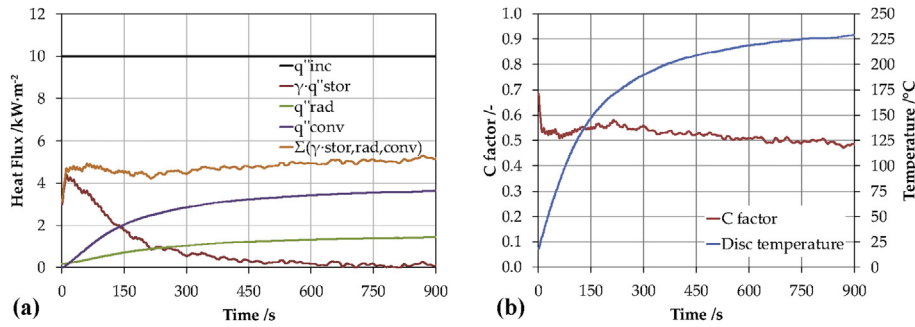


Fig. 7. (a) Time-history of the terms for the energy balance and (b) time-history of the calculated correction factor and disc temperature for a constant incident radiant heat flux of 10 kW m⁻².

store heat flux represents the biggest contribution to the energy balance, while the radiative and convective fluxes have a lower contribution. Once the quasi-steady state is achieved, the contribution from the stored heat flux is minor while the convective and radiative heat flux represent the biggest contribution. The sum of these terms determines the evolution of the conductive heat flux, which is expected not to be constant during the constant step of radiant heat flux. Therefore, the correction factor is expected to experience a variation with temperature for the same incident radiant heat flux. This is represented in Fig. 7a for a constant incident radiant heat flux of 10 kW m⁻².

As shown in Fig. 7b, this temperature dependency for a constant heat flux represents a short transient state, with the correction factor achieving an approximate constant value for the quasi-steady state. Then, it can be assumed a constant correction factor for a given range of temperatures, determined by the resolution of the steps of radiant heat flux selected for calibration. The correction factor is thus proposed to be selected from data points during the quasi-steady state.

Nonetheless, if this approach is used, an underestimation of the calculated incident radiant heat flux is expected during early stages of the transient state. A compensation factor γ is then proposed for correcting the term stored heat flux so as to compensate this underestimation during the transient-state, thus achieving a flat effective conductive heat flux. Therefore, the correction factor can be defined as:

$$C(T_{disc}) = \frac{\alpha_{disc} \cdot \dot{q}''_{inc} - [\gamma \cdot \dot{q}''_{stor,disc}(T_{disc}) + E_{disc}(T_{disc}) - \dot{q}''_{conv}(T_{disc})]}{\alpha_{disc} \cdot \dot{q}''_{inc}} \quad (17)$$

5.1. Calibration outcomes

Fig. 8 shows the temperature of the disc for two TSCs and different calibrations. Results indicate a good repeatability, although for the calibration TSC1.2 results are slightly lower during the calibration at lower heat fluxes, probably due to a slight misalignment between radiant panels and sample.

Table 2 presents the parameters used for the determination of the correction factor. For simplicity the absorptivity is assumed as unity, while the specific heat capacity and emissivity are assumed as the values obtained from the literature, which were previously presented in Table 1. A compensation factor for the transient state (γ) is chosen so as to obtain a low variation of the correction factor for each step of incident radiant heat flux. The selected characteristic length corresponds to the diameter of the metallic disc.

Fig. 9 shows the breakdown of the different energy terms obtained by calibration. It is observed that the sum of stored, radiative and convective flux follows an approximately constant value for each step of incident radiant heat flux, with a larger discrepancy for high heat fluxes such as 80 and 90 kW m⁻² indicating an expected worse correlation.

As a result, the corresponding correction factor defined as a function of the metallic disc temperature is presented in Fig. 10. It is observed a clear linear trend of the correction factor, despite the trend for the range at 20 kWm⁻² is slightly displaced to lower values. The peaks observed in Fig. 10 correspond to the first seconds after the transition from H-TRIS to a new heat flux value to be calibrated. These peaks are obtained due to the assumption that the incident heat flux provided by H-TRIS is a step function, while this is not actually the case. Therefore, they should be disregarded for defining the correlation between the correction factor and temperature.

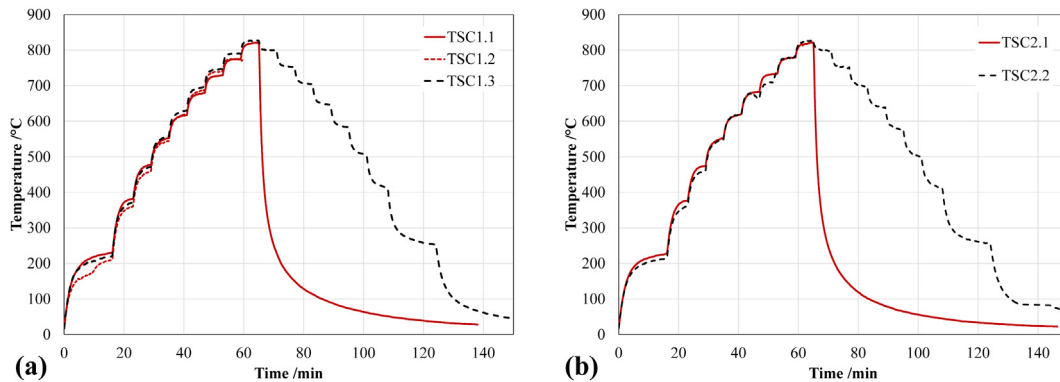


Fig. 8. Measured TSC temperature for the prescribed incident radiant heat flux - time curve. (a) TSC 1 (b) TSC 2.

Table 2
Parameters used for the calibration of the C factor.

Radiation absorption	Heat storage			Radiation emission	Convection
Absorptivity α /-	Transient compensation γ /-	Areal density m_{disc}/S_{disc} /kg m ⁻²	Specific heat capacity c_p /J kg ⁻¹ K ⁻¹ (T in °C)	Emissivity ϵ /-	Characteristic length L_c /m
1	0.8	9.532	$450 + 0.28 T - 2.91 \cdot 10^{-4} T^2 + 1.34 \cdot 10^{-3} T^3$	0.4	0.0096

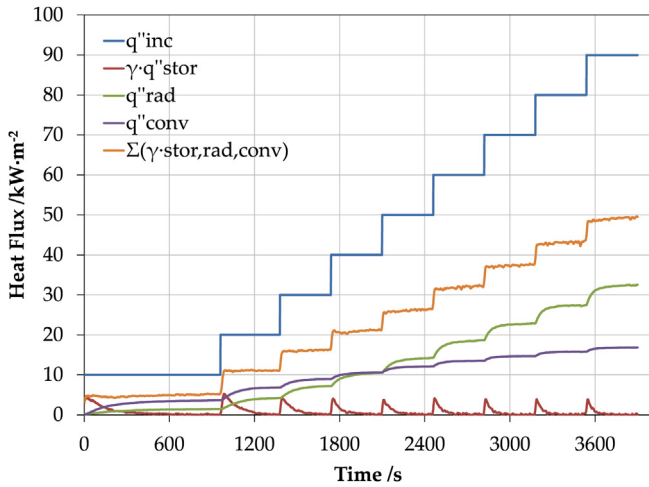


Fig. 9. Energy terms from the heat balance as noted in Eq. (4) for the calibration.

6. Experimental validation

A series of time-histories of incident radiant heat flux are imposed to a TSC in order to assess the effectiveness of the approach proposed by the authors, and to evaluate the discrepancy between the actual and calculated radiant heat flux considering the correction factor as noted in Fig. 10. The time dependent incident radiant heat flux is achieved by using H-TRIS, which is calibrated to provide different heat flux as a function of the relative distance between the target and the panels.

The prescribed histories of radiant heat flux are designed considering four steps, expected from a typical compartment fire, such as incipient phase, fire growth, fully-developed fire and decay [39]. These stages are defined as (1) constant radiant flux at

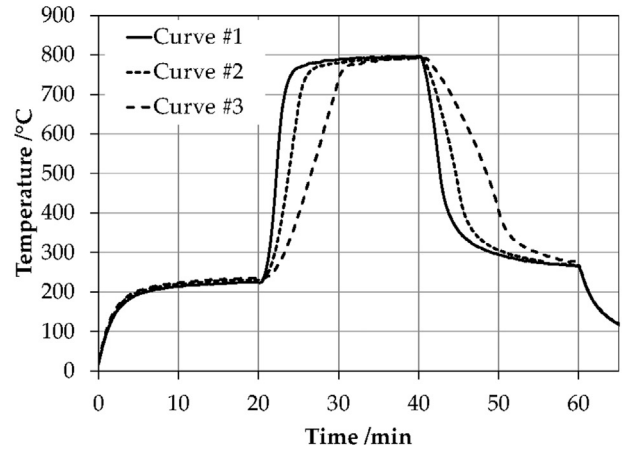
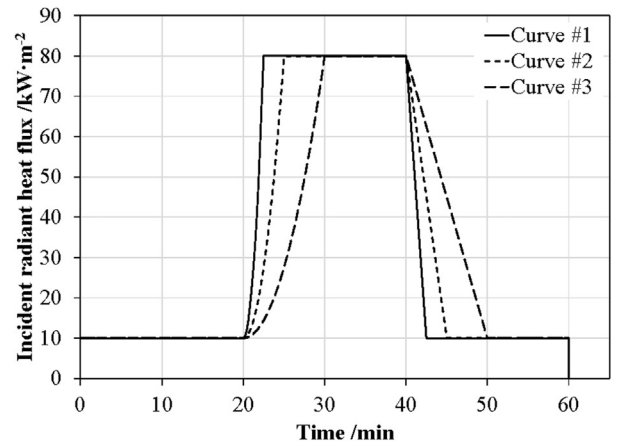


Fig. 11. (a) Prescribed incident radiant heat flux – time curves for three case studies (b) Temperature evolution of the metallic disc of the TSC for the three case studies.

10 kW m⁻², (2) growth as a t-squared function, (3) constant radiant flux at 80 kW m⁻² and (4) a linear decay. The three prescribed histories of incident radiant heat flux, which are presented in Fig. 11a, present differences in the rate of growth and decay, while the initial and the maximum heat flux are common. The resulting time-history of the temperature evolution of the metallic disc for these three cases is presented in Fig. 11b.

Figs. 12–14 show the prescribed (dashed line) and calculated curves (solid line) of incident radiant heat flux for the three cases being assessed. The calculated incident radiant heat flux curves are obtained by considering the parameters as shown in Table 2, the correction factor as a temperature function presented in Fig. 10 and Eq. (18) below:

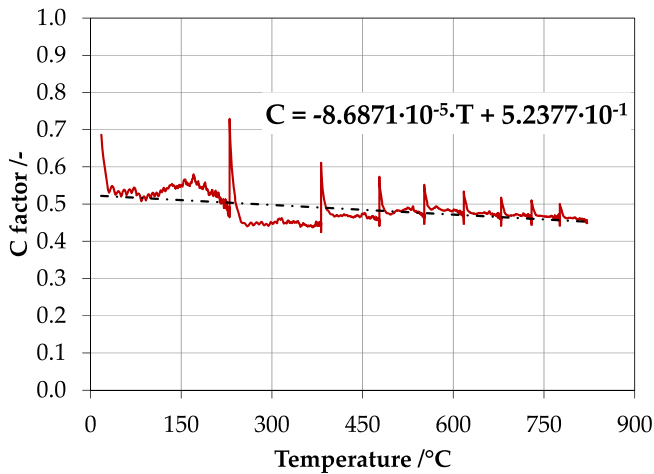


Fig. 10. Correlated correction factor as a temperature function.

$$\dot{q}''_{inc}(T_{disc}) = \frac{1}{\alpha_{disc} \cdot (1 - C)} \cdot \left[\gamma \cdot \frac{m_{disc}}{S_{disc}} \cdot c_p \cdot \frac{dT_{disc}}{dt} + \epsilon_{TSC} \cdot \sigma \cdot T_{disc}^4 + h_c \cdot (T_{disc} - T_{\infty}) \right] \tag{18}$$

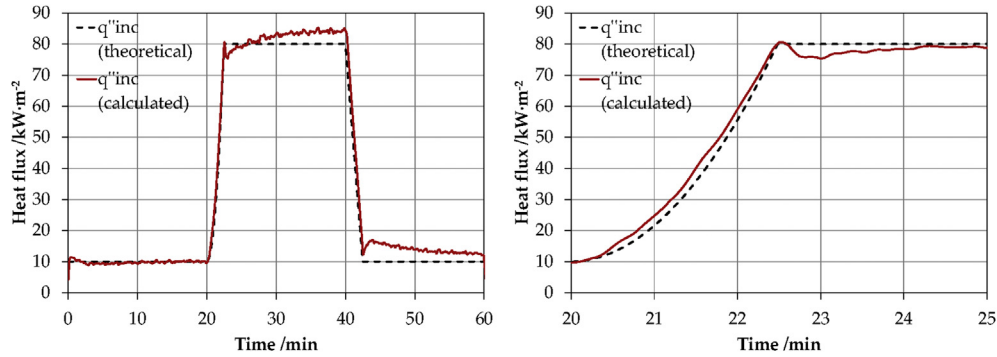


Fig. 12. Calibrated (red-solid) and calculated (black-dashed) incident radiant heat flux – time curves (case 1). (For interpretation of the references to colour in this figure legend, the reader is referred to the web version of this article.)

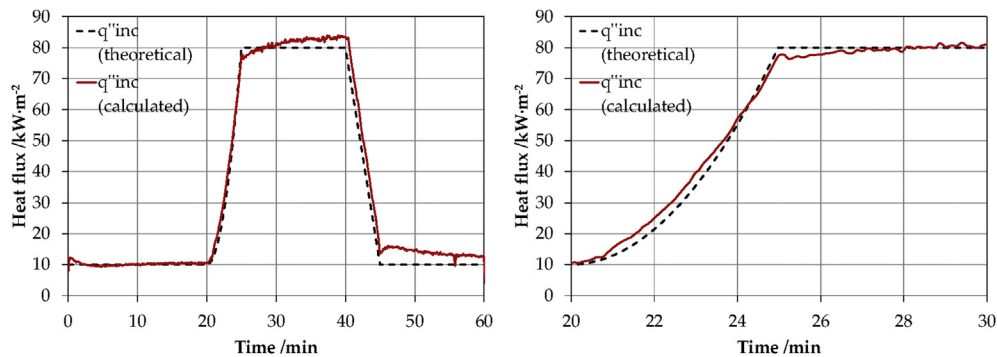


Fig. 13. Calibrated (red-solid) and calculated (black-dashed) incident radiant heat flux – time curves (case 2). (For interpretation of the references to colour in this figure legend, the reader is referred to the web version of this article.)

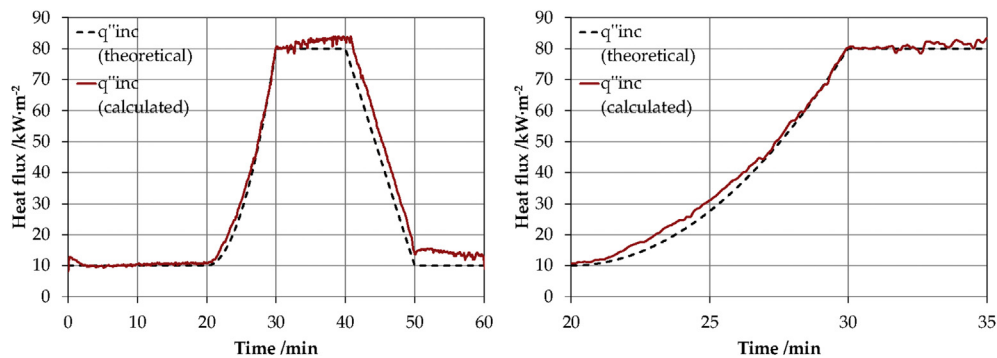


Fig. 14. Calibrated (red-solid) and calculated (black-dashed) incident radiant heat flux – time curves (case 3). (For interpretation of the references to colour in this figure legend, the reader is referred to the web version of this article.)

In general, a good agreement is observed between the prescribed and calculated flux for the three study cases proposed. The steady state of 10 kW m^{-2} is well replicated, with a slight overestimating peak in the first minute due to overestimation of the conductive flux that the correction factor provides during early stages of the transient state as shown in previous sections. The growth of incident radiant heat flux as a t -square is reasonably well captured, with a slight overestimation of maximum 4 kW m^{-2} as shown in Fig. 15, which presents the residues between the theoretical and calculated heat flux curves. During the third step with a constant heat flux of 80 kW m^{-2} , the calculated incident radiant heat flux provides a worse estimation than for the first step with a constant heat flux of 10 kW m^{-2} . Yet, the accuracy of the result is reasonably good, with a maximum residue of 5 kW m^{-2} . The fourth

step, represented as a cooling phenomenon, provides similar results, although better accuracy is found for the case 1 (fastest cooling) than the case 3 (slowest cooling). The final steady-state step is the region worst replicated by the *a posteriori* analysis, likely due to the inversion of the conductive heat flow between the disc and insulation core, which has not been considered. This will be properly investigated in future work.

7. Concluding remarks

This paper presents a novel method for the quantification of irradiance at gas – solid phase boundaries during exposure to real fires. The presented methodology enables the spatial characterisation of irradiance from sensors positioned at multiple locations

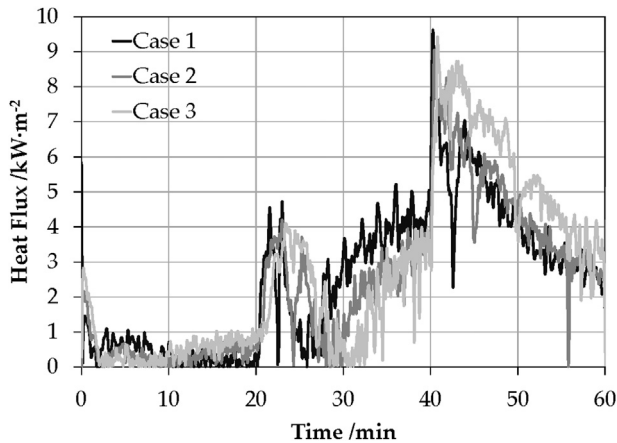


Fig. 15. Residues from calibrated and calculated incident radiant heat flux for the three case studies.

over surfaces of interest that are exposed to the effects of real fires. Indeed, this method was specifically developed due to the need for distributed measurement of irradiance to spatially characterise the boundary condition over the course of multiple large-scale experiments.

This requirement necessitated low cost, rapidly reproducible devices. By necessity therefore, these gauges, and thus also the measurements made, are designed to be simple. While reasonably robust, the low cost of production also enables rapid and simple replacement of broken gauges. The calibration methodology presented in detail here is designed to account for the uncertainties associated to the simplicity of the measurement technique and enables an estimation of the typical error bars associated to the output from this technique. By describing the calibration process in detail, it is intended that others will be able to adapt the underlying premise to the specific needs of other experiments enabling the use of different material properties and dimensions following the performance of an appropriate calibration. An advantage from TSCs over the other instruments used to quantify incident radiant heat flux during fire tests is its relative inexpensive cost of fabrication. Additionally, the instrument may survive after a fire experiment if it is designed properly, giving the possibility of test repeats.

An experimental validation under cooling conditions by natural convection has been performed for the described design using H-TRIS to reproduce three types of dynamic irradiation curves. The experimental results, consisting of thermal evolution of the TSC metallic disc from the different study cases, have been processed using the calibrated correction factor. *A posteriori* results provide a good estimation of the heating periods, with a maximum deviation of 5 kW m^{-2} for all of the cases studied. For the cooling phase, the maximum deviation between the *a posteriori* calculation of incident radiant heat flux and the nominal heat flux imposed by the radiant panels is a max of 9 kW m^{-2} . In general therefore, the trend obtained by the *a posteriori* analysis provides good trends of the nominal irradiation for all of the trialled irradiation exposures. However, future work is still required in order to verify the methodology in conditions of heating by convection, and a better estimation of the convective heat transfer coefficient.

Acknowledgements

The work presented herein was developed as part of the 'Real Fires for the Safe Design of Tall Buildings' project, which is an EPSRC funded project (Grant No. EP/J001937/1). The authors are extremely grateful to EPSRC for funding this project. The authors would also

like to gratefully acknowledge funding contribution from Rockwool International A/S towards the Ph.D. studies of Juan P. Hidalgo, during which this work was mainly developed. The authors would also like to acknowledge Eric Mueller for his contribution.

References

- [1] Pettersson O. Need for and some remarks on internationally standardized fire test procedures. Lund, Sweden: Lund Institute of Technology; 1973. 19 pp.
- [2] SFPE. Sipe engineering guide to fire exposure of structural elements. USA: Society of Fire Protection Engineers; 2004.
- [3] Stern-Gottfried J, Rein G. Travelling fires for structural design-Part I: literature review. *Fire Saf J* 2012;54:74–85. <http://dx.doi.org/10.1016/j.firesaf.2012.06.003>.
- [4] Torero JL, Majdalani AH, Abecassis-Empis C, Cowlard A. In: Revisiting the compartment fire, 11th international symposium on fire safety science; 2014.
- [5] Bailey CG, Burgees IW, Plank RJ. Computer simulation of a full-scale structural fire test. *Struct Eng* 1996;74(6):93–100.
- [6] Stern-Gottfried J, Rein G. Travelling fires for structural design-Part II: design methodology. *Fire Saf J* 2012;54:96–112. <http://dx.doi.org/10.1016/j.firesaf.2012.06.011>.
- [7] Welch S, Jowsey S, Deeny S, Morgan R, Torero JL. BRE large compartment fire tests—Characterising post-flashover fires for model validation. *Fire Saf J* 2007;42(no. 8):548–67. <http://dx.doi.org/10.1016/j.firesaf.2007.04.002>.
- [8] Bisby L, Gales J, Maluk C. A contemporary review of large-scale non-standard structural fire testing 2013;2(no. 1):27. <http://dx.doi.org/10.1186/2193-0414-2-1>.
- [9] Incropera FP, DeWitt D, Bergman TL, Lavine AS. Principles of heat and mass transfer. seventh ed. John Wiley & Sons, Inc.; 2011.
- [10] Carslaw HS, Jaeger JC. Conduction of heat in solids. 2th ed 1986.
- [11] Jowsey A. Fire imposed heat fluxes for structural analysis. The University of Edinburgh; 2006. Ph.D. thesis.
- [12] Blevins LG, Pitts WM. Modeling of bare and aspirated thermocouples in compartment fires. *Fire Saf J* 1999;33:239–59. [http://dx.doi.org/10.1016/S0379-7112\(99\)00034-x](http://dx.doi.org/10.1016/S0379-7112(99)00034-x).
- [13] Stern-Gottfried J, Rein G, Bisby LA, Torero JL. Experimental review of the homogeneous temperature assumption in post-flashover compartment fires. *Fire Saf J* 2010;45:249. <http://dx.doi.org/10.1016/j.firesaf.2010.03.007>.
- [14] Hidalgo JP, Cowlard A, Abecassis-Empis C, Maluk C, Majdalani AH, Kahrmann S, et al. An experimental study of full-scale open floor plan enclosure fires. *Fire Saf J* 2016 (in press).
- [15] Cowlard A. Sensor and model integration for the rapid prediction of concurrent flow flame spread. The University of Edinburgh; 2009. Ph.D. thesis. <http://hdl.handle.net/1842/2753>.
- [16] Amundarain A. Assesment of the thermal efficiency, structure and fire resistance of lightweight building systems for optimised design. The University of Edinburgh; 2007. Ph.D. thesis. <http://hdl.handle.net/1842/2128>.
- [17] Gollner MJ. Studies on upward flame spread. The University of California; 2012. Ph.D. thesis.
- [18] Abecassis-Empis C, Reszka P, Steinhaus T, Cowlard A, Biteau H, Welch S, et al. Characterisation of dalmarnock fire test one. *Exp Therm Fluid Sci* 2008;32(no. 7):1334–43.
- [19] Gardon R. An instrument for the direct measurement of intense thermal radiation. *Rev Sci Instrum* 1953;24:366–70.
- [20] Lattimer BY, Diller TE. Quantifying thermal boundary condition details using a hybrid heat flux gage. *Fire Saf Sci* 2011:987–1000. <http://dx.doi.org/10.3801/IAFSS.FSS.10-987>.
- [21] Wickström U, Wetterlund I. Total heat flux cannot be measured. *Interflam*. 2014. p. 269–76.
- [22] ASTM E457. Standard test method for measuring heat-transfer rate using a thermal capacitance (slug) calorimeter. 2015.
- [23] ASTM E458. Standard test method for heat of ablation. 2015.
- [24] ASTM E3507. Standard test method for measuring heat flux using directional flame thermometers with advanced data analysis techniques. 2015.
- [25] Kidd CT, Nelson CG. How the Schmidt-Boelter gage really works. In: Proceedings 41st international instrumentation symposium. Research Triangle Park, NC: ISA; 1995. p. 347–68.
- [26] Filtz JR, Lièvre M, Valin T, Hameury J, Wetterlund I, Persson B, et al. Improving Heat Flux Meter Calibration for Fire Testing Laboratories (HFCAL). Technical report elaborated for the Direction Générale des Affaires Economiques et Financières, Brussels, France. 2002. p. 121.
- [27] Bryant R, Womeldorf C, Johnsson E, Ohlemiller T. Radiative heat flux measurement uncertainty. *Fire Mater* 2003;27:209–22. <http://dx.doi.org/10.1002/fam.822>.
- [28] ASTM E459. Standard test method for measuring heat transfer rate using a thin-skin calorimeter. 2011.
- [29] Alston JJ. Room/Corner fire calibration data: marine composite screening specimens. Worcester Polytechnic Institute (USA); 2004 (M.Sc. thesis).
- [30] Beji T, Verstockt S, Merci B, Abecassis-Empis C, Krajcovic M, Majdalani A. RABOT2012 – enclosure effects on flame spread over a sofa and consequences on the fire development. In: Proceedings of the seventh international seminar fire and explosion hazards; 2013. http://dx.doi.org/10.3850/978-981-07-5936-0_039.

- [31] Shaw T, Gibson T, Karlovsek J, Emberley R, Torero JL. Experimental evaluation of the heat flux induced by tunnel fires. *Tunn Undergr Space Technol* 2015;60: 49–55. <http://dx.doi.org/10.1016/j.tust.2016.07.015>.
- [32] Mueller E, Skowronski N, Clark K, Gallagher M, Kremens R, Thomas JC, et al. Localized fire behavior regimes in a field scale experiment. In: *Proceedings 6th international fire ecology and management congress, San Antonio, TX, USA; 2015*.
- [33] Wickström U. Proposal regarding temperature measurements in fire test furnaces, SP-report 1986:17. Swedish National Testing Institute; 1986.
- [34] Ingason H, Wickström U. Measuring incident radiant heat flux using the plate thermometer. *Fire Saf J* 2007;42(no. 2):161–6. <http://dx.doi.org/10.1016/j.firesaf.2006.08.008>.
- [35] Maluk C, Bisby L, Krajcovic M, Torero JL. A heat-transfer rate inducing system (H-TRIS) test method. *Fire Saf J* 2016. <http://dx.doi.org/10.1016/j.firesaf.2016.05.001> (in press).
- [36] Lennon PF, Silcok GWH. An investigation of the ability of a thin plate heat flux device to determine the incident heat fluxes during enclosure fires. *Int J Eng Performance-Based Fire Codes* 2001;3(no. 1):1–15.
- [37] Hidalgo JP. Performance-based methodology for the fire safe design of insulation materials in energy efficient Buildings. The University of Edinburgh; 2015. Ph.D. thesis, <http://hdl.handle.net/1842/10601>.
- [38] Churchill SW, Chu HHS. Correlating equations for laminar and turbulent free convection from a vertical plate. *Int J Heat Mass Transf* 1975;18(no. 11): 1323–9. [http://dx.doi.org/10.1016/0017-9310\(75\)90243-4](http://dx.doi.org/10.1016/0017-9310(75)90243-4).
- [39] Drysdale D. *An introduction to fire dynamics*. third ed. John Wiley & Sons, Ltd.; 2011.